Supporting Information

Skeletal Octahedral Nanoframe with Cartesian Coordinates *via* Geometrically Precise Nanoscale Phase Segregation in a Pt@Ni Core-Shell Nanocrystal

Aram Oh,[†,⊥] Hionsuck Baik,[††,‡] Dong Shin Choi,[§,‡] Jae Yeong Cheon,[∥,‡] Byeongyoon Kim,[†,⊥] Heejin Kim,[§] Seong Jung Kwon,[#] Sang Hoon Joo,*[,∥,¶] Yousung Jung*[,§] and Kwangyeol Lee*[,†,⊥]

[†]Center for Molecular Spectroscopy and Dynamics, Institute for Basic Science (IBS), Korea University, Seoul 136-713, Republic of Korea

[⊥]Department of Chemistry and Research Institute for Natural Sciences, Korea University, Seoul 136-713, Republic of Korea

[††]Korea Basic Science Institute (KBSI), Seoul 136-713, Republic of Korea

[§]Graduate school of Energy Environment Water and Sustainability (EEWS), Korea Advanced Institute of Science and Technology (KAIST), Daejeon 305-701, Republic of Korea

[∥]Department of Chemistry, Ulsan National Institute of Science and Technology (UNIST), Ulsan 689-798, Republic of Korea

[¶]School of Energy and Chemical Engineering, Ulsan National Institute of Science and Technology (UNIST), Ulsan 689-798, Republic of Korea

[#]Department of Chemistry, Konkuk University, Seoul 143-701, Republic of Korea

*To whom all correspondence should be addressed to K. L. (email: kylee1@korea.ac.kr), Y. J. (email: ysjn@kaist.ac.kr) and S. H. J. (email: shjoo@unist.ac.kr)

[‡]These authors contributed equally to this work.

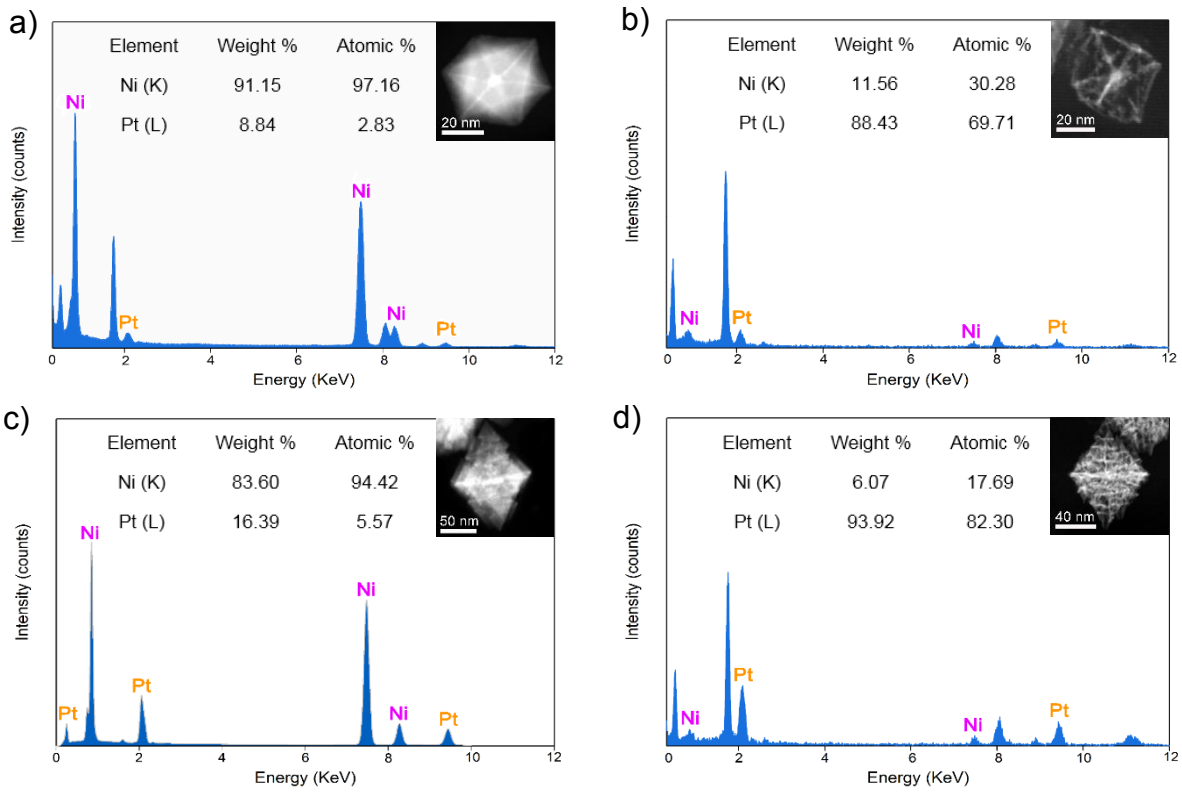

Figure S1. Quantitative EDS analysis of phase-segregated nanoparticles. Quantitative EDS analysis of (a) PON, (b) OSN, (c) PHN, and (d) HSN, respectively. While (a) PON and (c) PHN, the original synthetic products, exhibit the Ni content as the major component in the phase-segregated nanostructure, Pt becomes the major component for (b) OSN and (d) HSN after chemical etching process. The non-marginal presence of Ni component in the final etched products of PHN and HSN indicates the formation of Pt-rich PtNi alloy, likely Pt/Ni solid solution, structures.

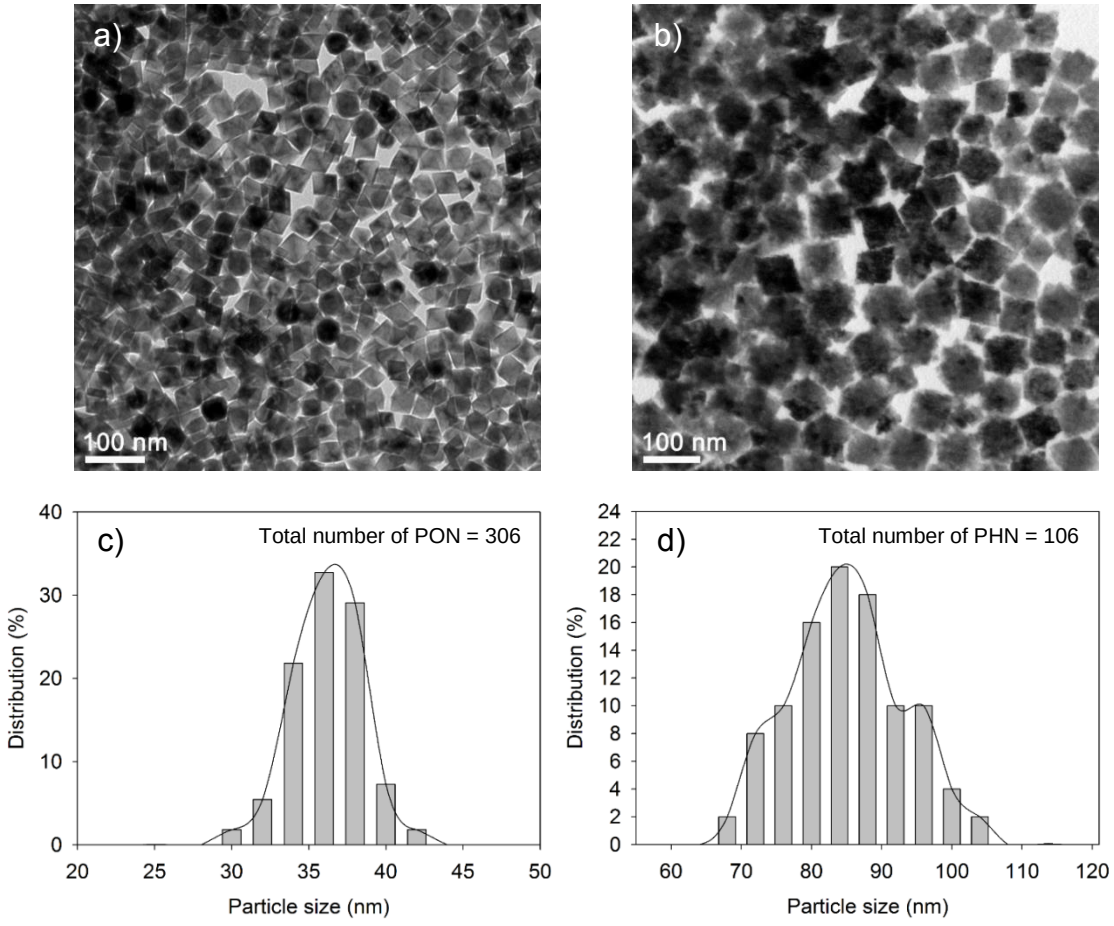

Figure S2. TEM images of nanoparticles [PON in (a) and PHN in (b)] and their respective histograms (c and d) for particle size distributions. PON shows a narrow size distribution mainly from 34 to 38 nm and PHN exhibits a broader distribution mainly from 70 to 100 nm.

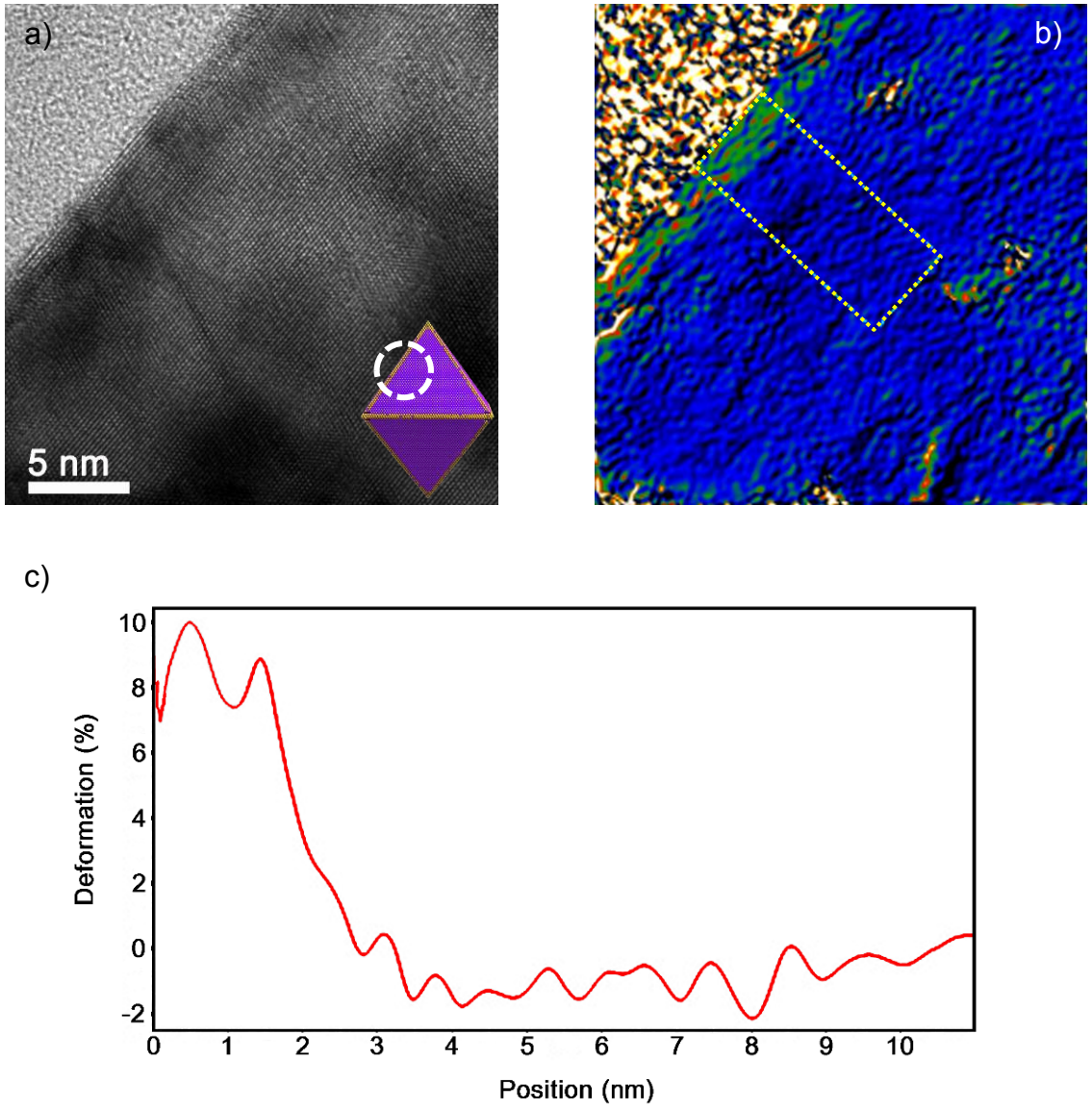

Figure S3. Lattice deformation of PON by Geometric Phase Analysis (GPA). (a) HRTEM image of <110> edge of PON, corresponding to the white dashed circle in the inset model, (b) strain map extracted from GPA for (111) plane and (c) strain profile obtained from GPA strain map. The strain profile shows approximately 10 percent of dilatation in the side wall (about 5~6 lattice from the surface) to inside of the octahedral nanostructure.

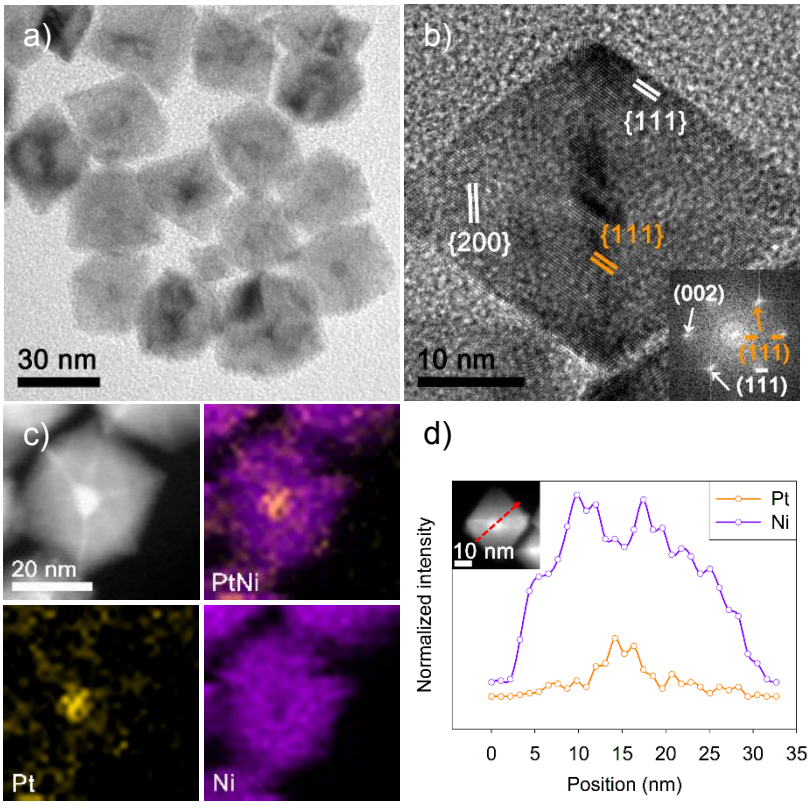

Figure S4. Structure and component analysis of PON at 165 minute. (a) TEM image, (b) HRTEM spatial resolution analysis, (c) EDS elemental mapping and (d) line profile analysis of PON show three Pt-rich inner axes and core separated from Ni domain octahedral nanoparticle, while the edges hardly exhibit any Pt component, for Pt diffusion along the <110> edges did not start at this point of the reaction. The orange and white marks in HRTEM image represent Pt (d_{111}= 2.26 Å) and Ni (d_{111}= 2.03 Å , d_{200}= 1.76 Å) along the <110> zone axis.

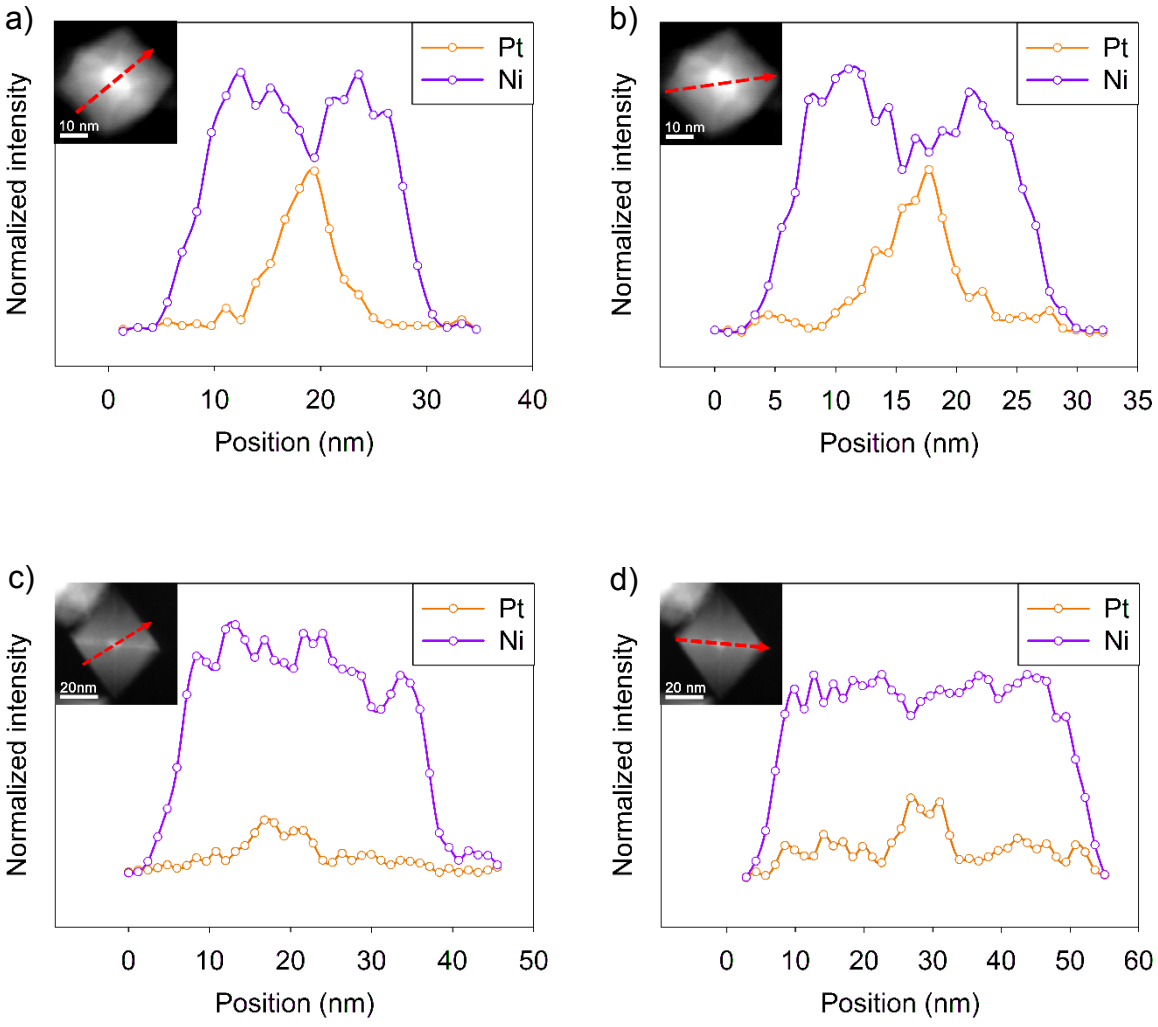

Figure S5. EDS line profiles with HAADF-STEM images of the reaction intermediate core-shell Pt@Ni octahedral nanoparticle and the final product phase-segregated octahedral PtNi nanoparticle. Line scanning for (a,b) intermediate core-shell nanostructure and (c,d) phase-segregated final structure was performed along different crystal directions. As the reaction proceeds, the Pt core size of nanostructure decreases and the Pt proportion in edges and axes increases. The red arrows in the insets of line profile images indicate line scan directions for the corresponding nanoparticles.

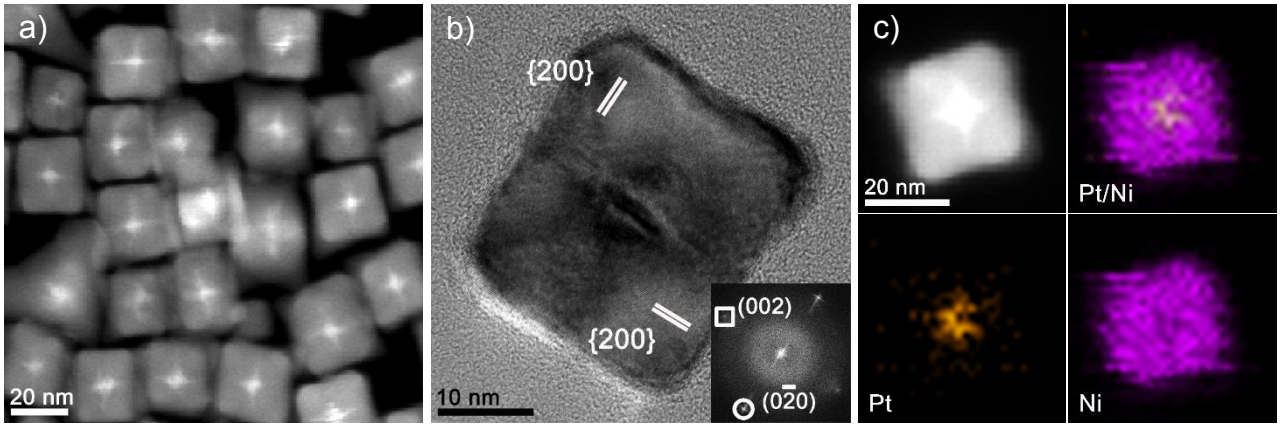

Figure S6. Structural analysis of core-shell Pt@Ni concave nanocube. (a) HAADF-STEM, (b) HRTEM and (c) EDS elemental mapping images of core-shell Pt@Ni concave nanocube. EDS mapping image shows the phase segregation between Pt core (orange) and Ni shell (purple) components. In (b), HRTEM image is shown with a FFT image along the <100> zone axis. Ni-rich phase in a concave nanocube can be confirmed through *d*-spacing analysis (Ni, d_{200}= 1.76 Å).

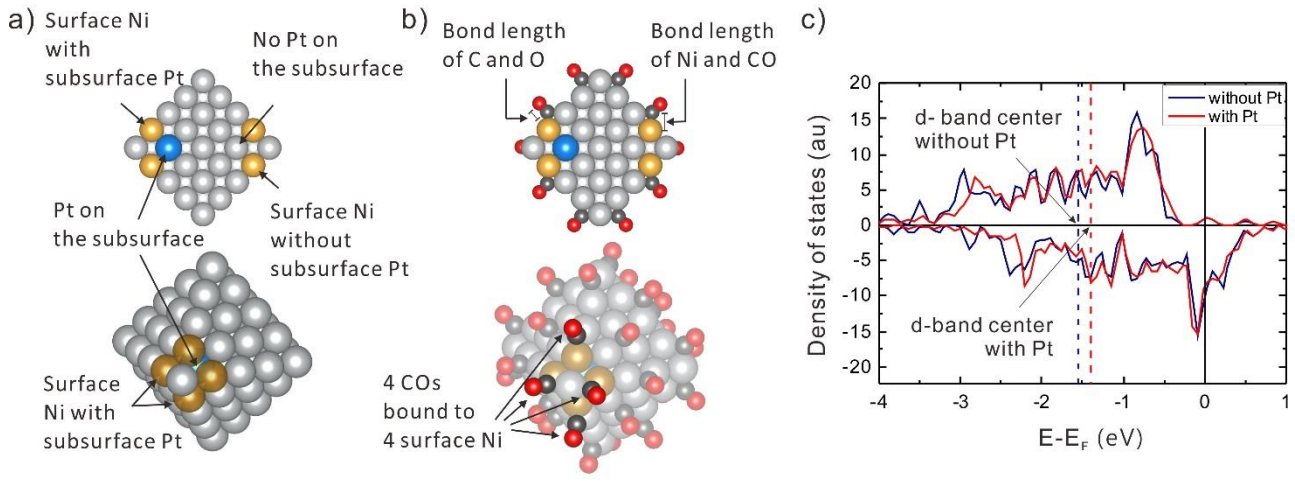

Figure S7. d-band center calculations for surface Ni atoms. (a) d-band center was considered for the 4 surface Ni atoms (yellow) with and without Pt (blue) on the subsurface layer. (b) Bond length of 4 CO molecules were considered which were bound to the 4 surface Ni atoms with and without Pt on the subsurface layer. Also, the bond length between the 4 Ni atoms and the 4 CO molecules were evaluated. (c) The density of states for the d-band in the 4 surface Ni atoms with and without Pt on the subsurface layer. The d-band center shifted upward in the presence of Pt from -1.52 eV to -1.44 eV.

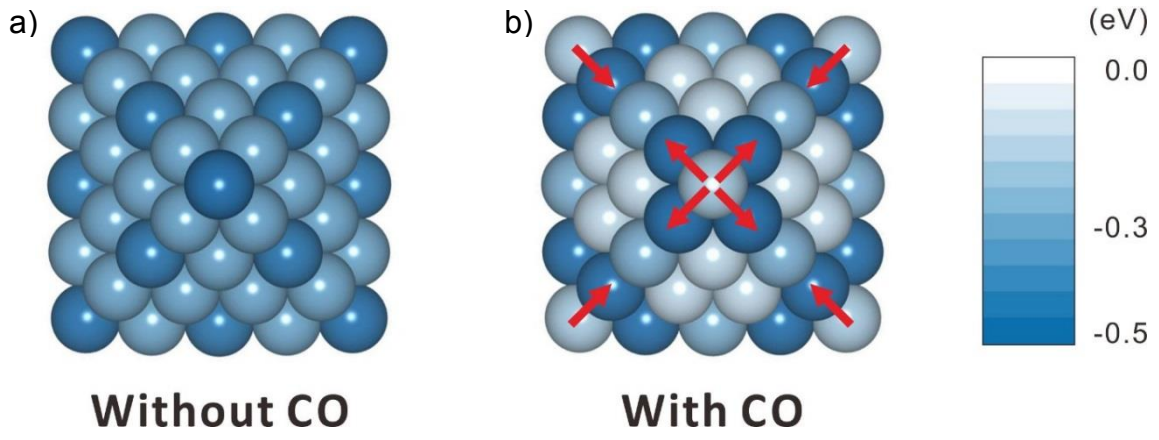

Figure S8. Relative energy of each position on the surface of Ni nanoparticle (a) without CO and (b) with CO. In the absence of CO, the vertex position has the lowest energy. However, the edge position which keeps the lowest energy results in the diffusion of the Pt along the edge (red arrow) after it segregates on the vertex in the presence of CO.

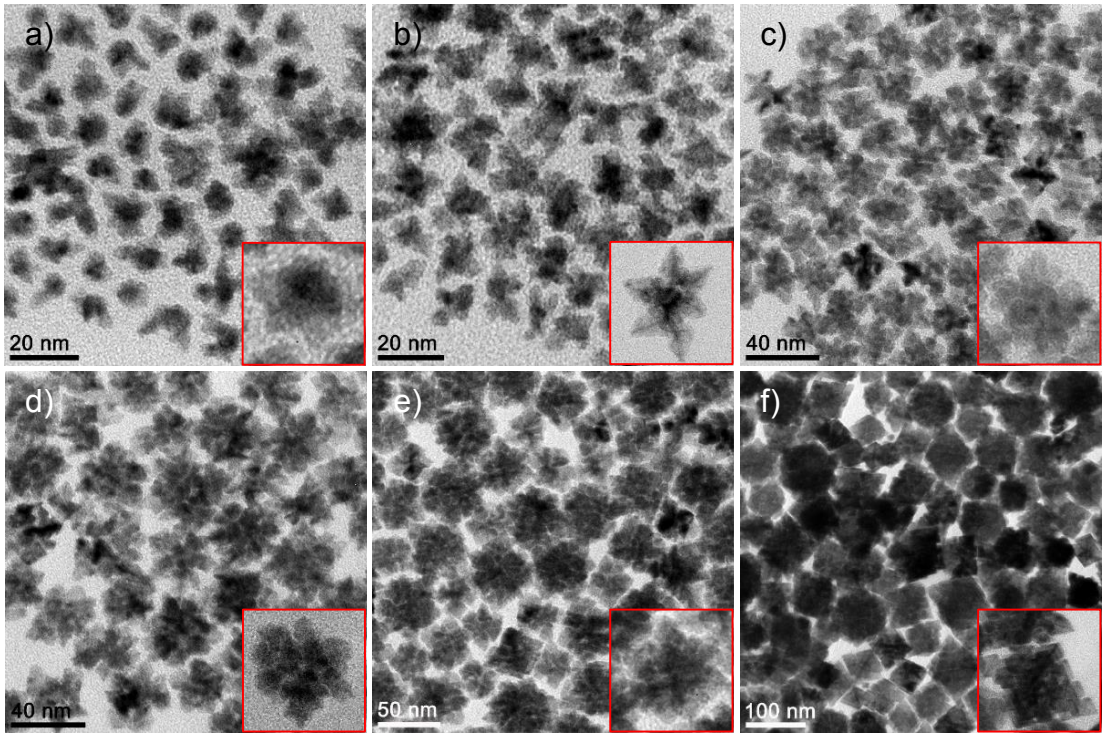

Figure S9. TEM images of intermediates, leading to the formation of PHN, at different reaction times: (a) 10 min, (b) 12 min, (c) 15 min, (d) 20 min, (e) 30 min, and (f) 300 min. In the initial stage, (a,b) the PtNi alloy nanoparticles with six branches are formed from poorly defined Pt-based seeds. (c) Each branch within the particle was further developed into new branches, which continued to grow. (d-f) Repetition of this process combined with growth of branches into small octahedrons eventually led to the formation of a dendritic nanostructure with an overall shape of octahedron.

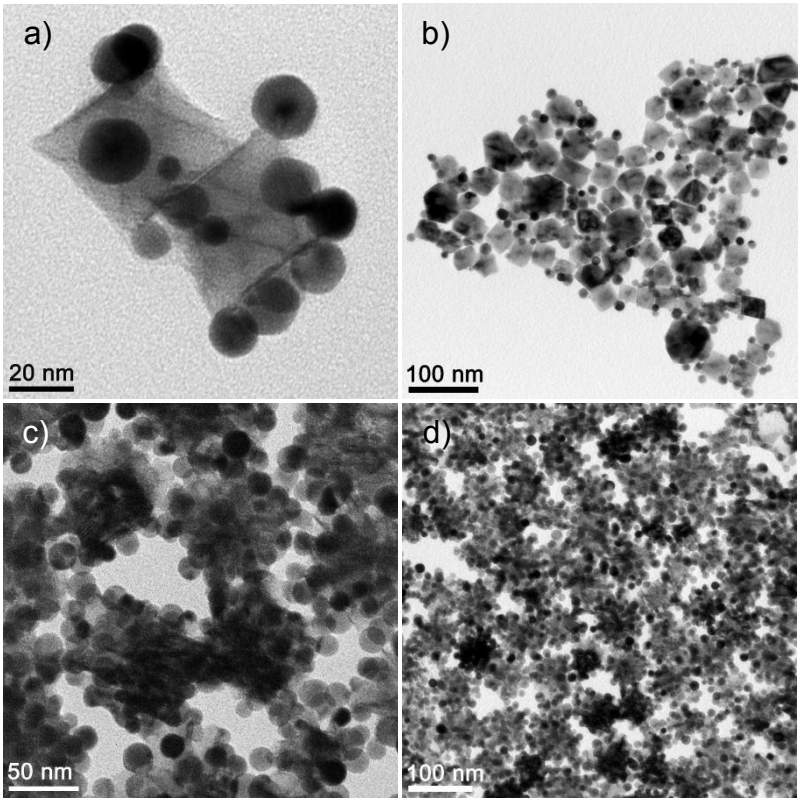

Figure S10. TEM images for Au overgrown phase-segregated PtNi nanoparticles. TEM images of (a,b) PON with Au nanoparticles grown and (c,d) PHN with Au nanoparticles grown. Au nanoparticles grew preferentially on the edges and vertices of phase-segregated PtNi nanocrystals, suggesting a high reactivity of these sites.

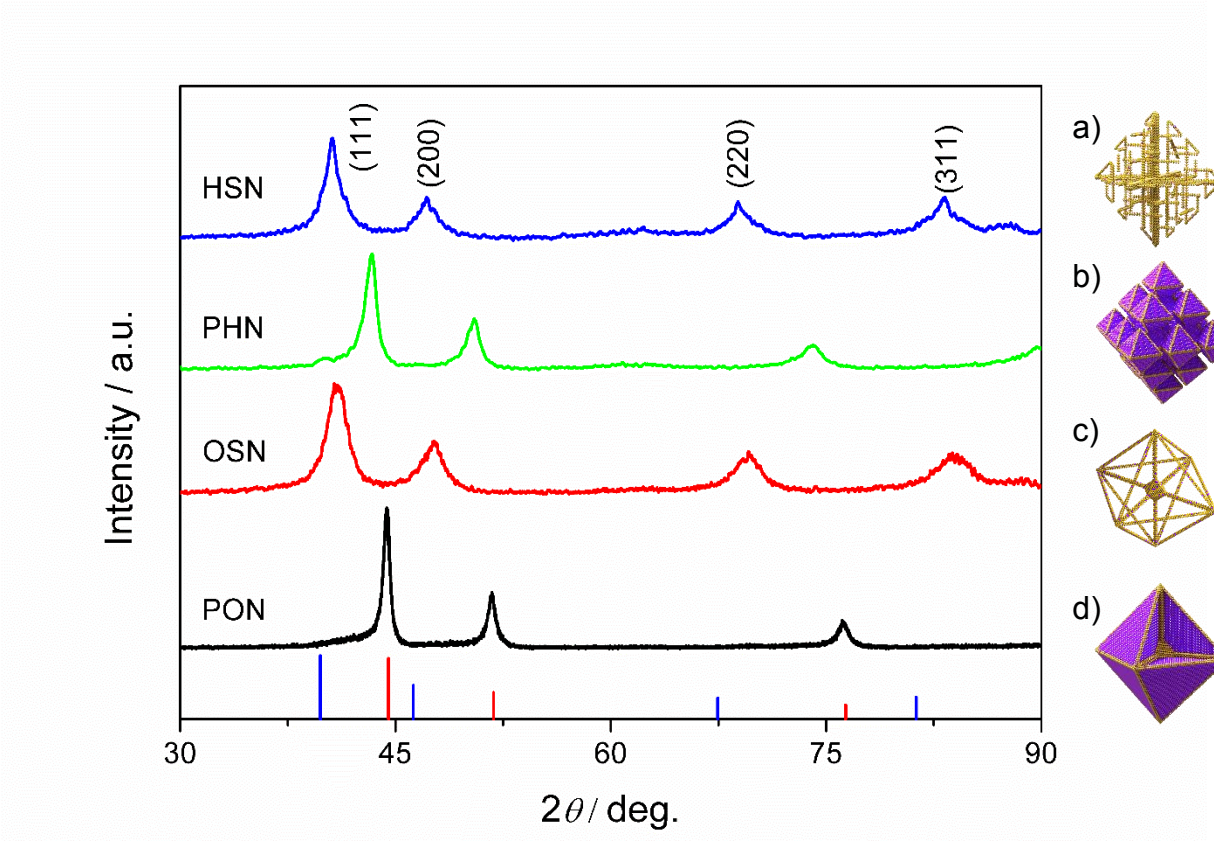

Figure S11. XRD patterns of phase-segregated nanoparticles indicate a face-centered cubic structure: (a) HSN, (b) PHN, (c) OSN, (d) PON. Color sticks indicate the reference X-ray diffraction lines: blue, Pt (JCPDS #04-0802), and red, Ni (JCPDS #04-0850).

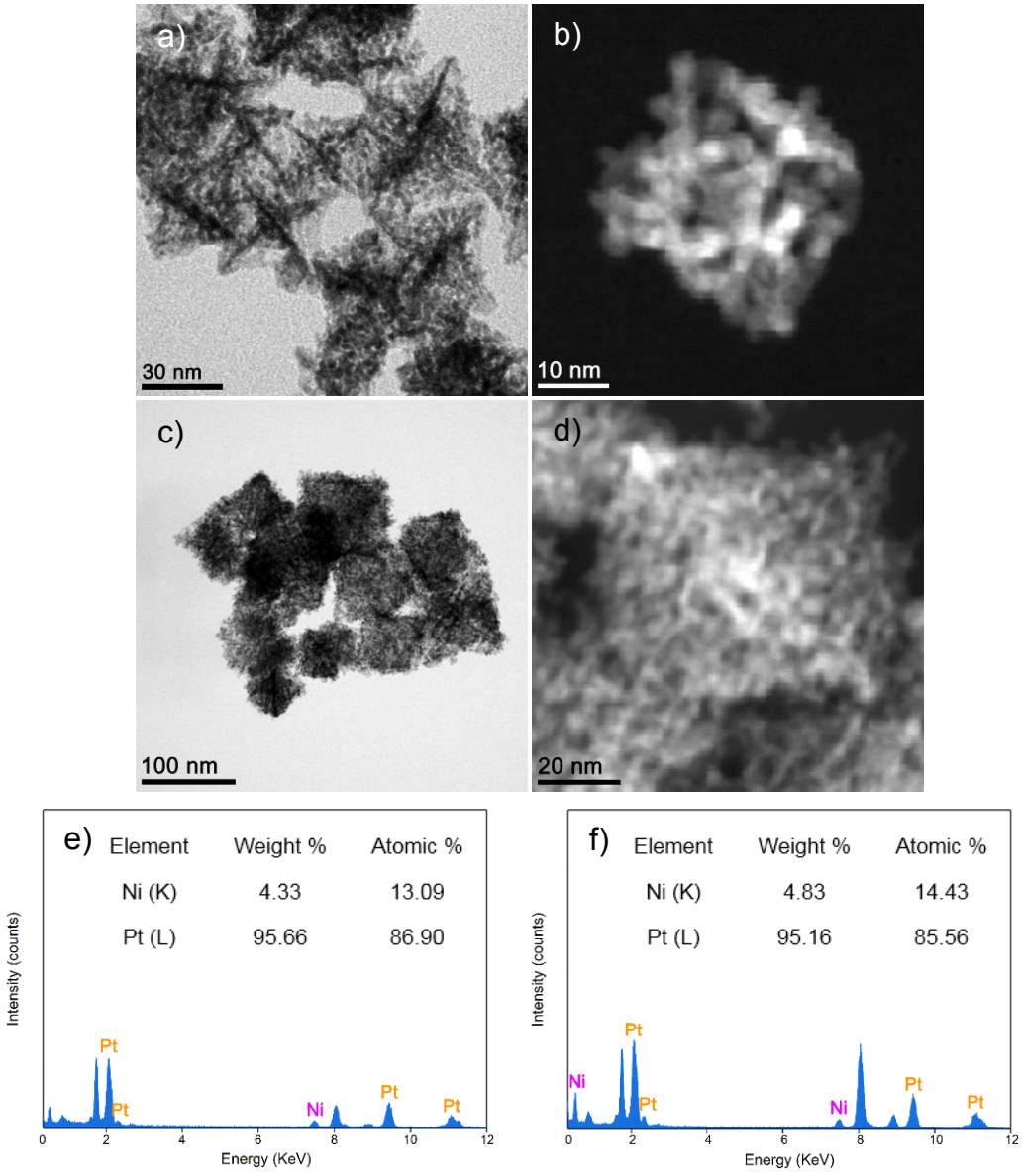

Figure S12. Structural analysis for nanoframes with overgrown Pt phase. TEM and HAADF-STEM images of (a,b) OSN_OV and (c,d) HSN_OV. Pt nanoparticles grew along the edges and vertices of skeletal Pt-based nanocrystals. EDS analysis of (e) OSN_OV and (f) HSN_OV.

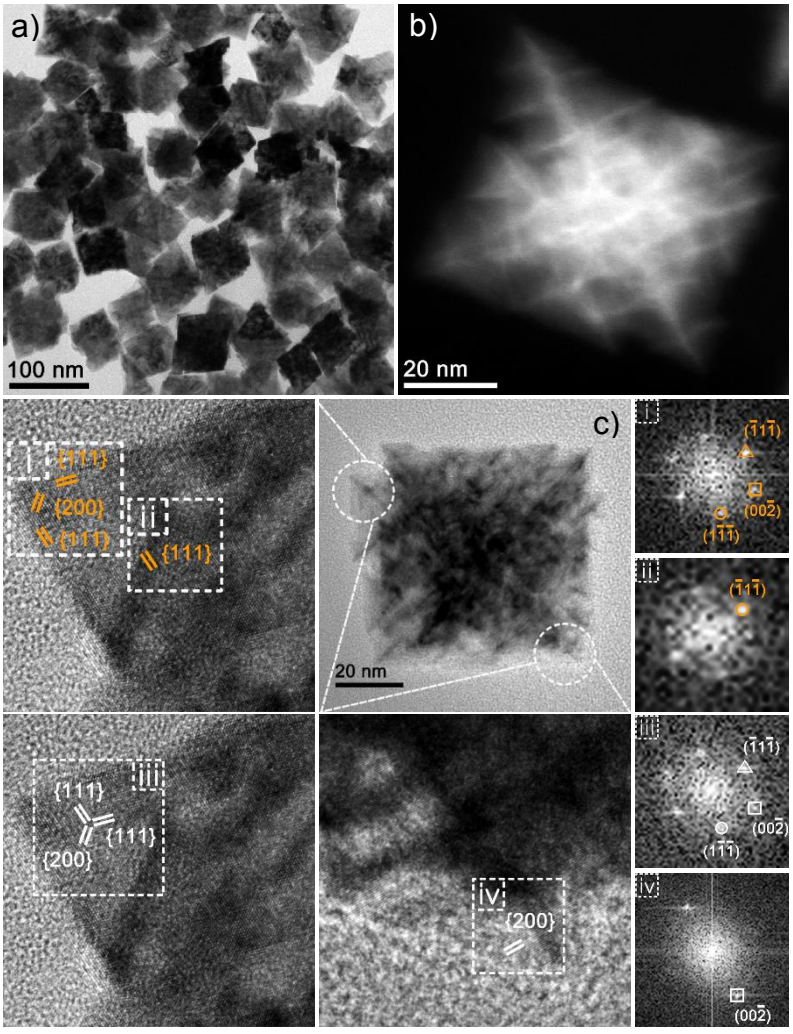

Figure S13. TEM analysis of PHN. (a) TEM, and (b) HAADF-STEM images of PHN. (c) HRTEM with FFT images of PHN along the <110> zone axis. The phase segregation between Pt-rich and Ni-rich phases in a small octahedral branch can be confirmed through *d*-spacing analysis. The orange and white marks in HRTEM and FFT images represent Pt (d_{111}= 2.26 Å , d_{200}= 1.96 Å) and Ni (d_{111}= 2.03 Å , d_{200}= 1.76 Å), respectively.

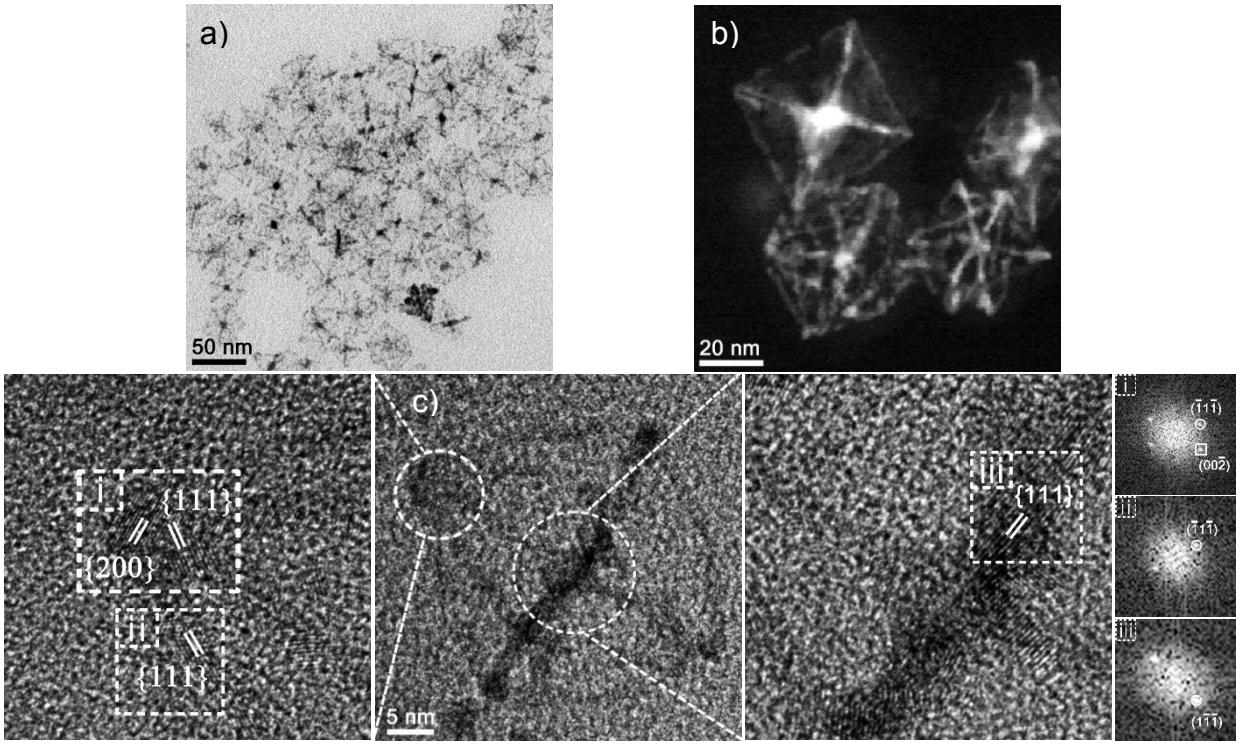

Figure S14. TEM analysis of OSN. (a) TEM, (b) HAADF-STEM, and (c) HRTEM images of OSN. The average thicknesses of edges and axes of OSN are 1.5 ± 0.2 nm and 1.8 ± 0.3 nm, respectively. The FFT images of OSN along the <110> zone axis are also shown (Pt, d_{111}= 2.26 Å , d_{200}= 1.96 Å).

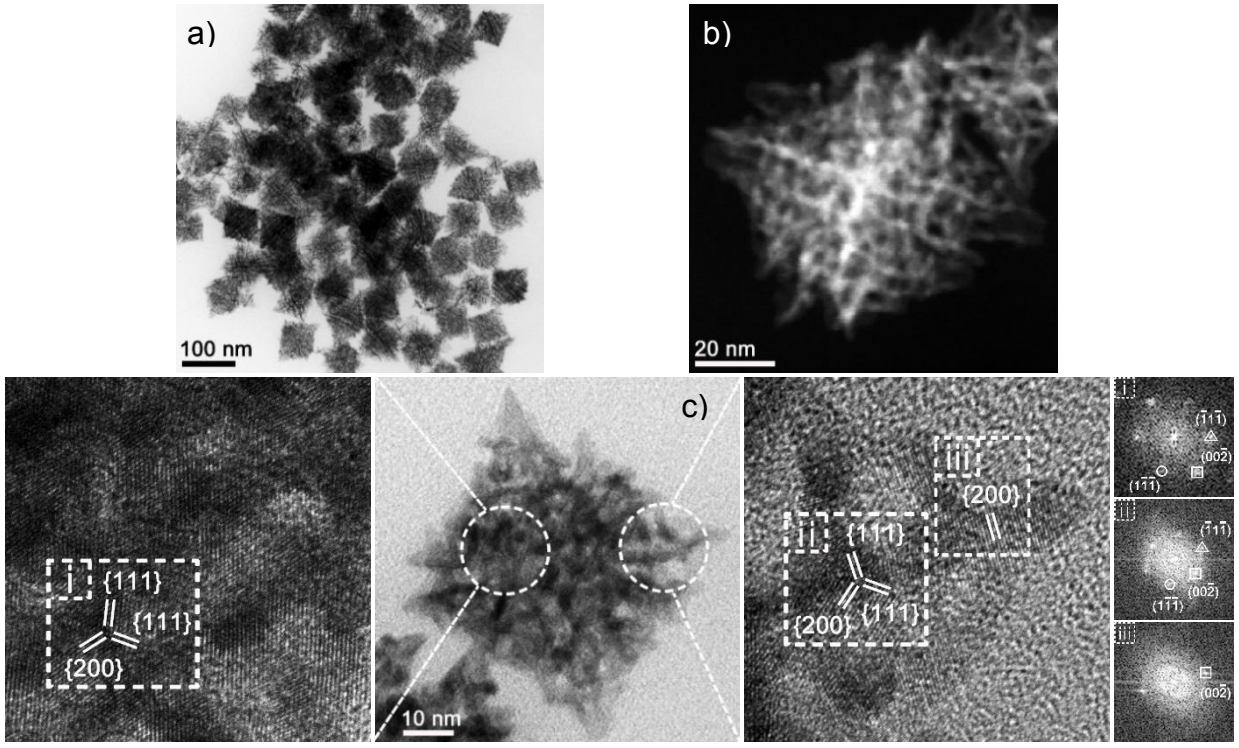

Figure S15. TEM analysis of HSN. (a) TEM, (b) HAADF-STEM, (c) HRTEM images of HSN. The average frame thickness is 3.9 ± 1.0 nm. The FFT images of HSN along the <110> zone axis are also shown (Pt, d_{111}= 2.26 Å , d_{200}= 1.96 Å)

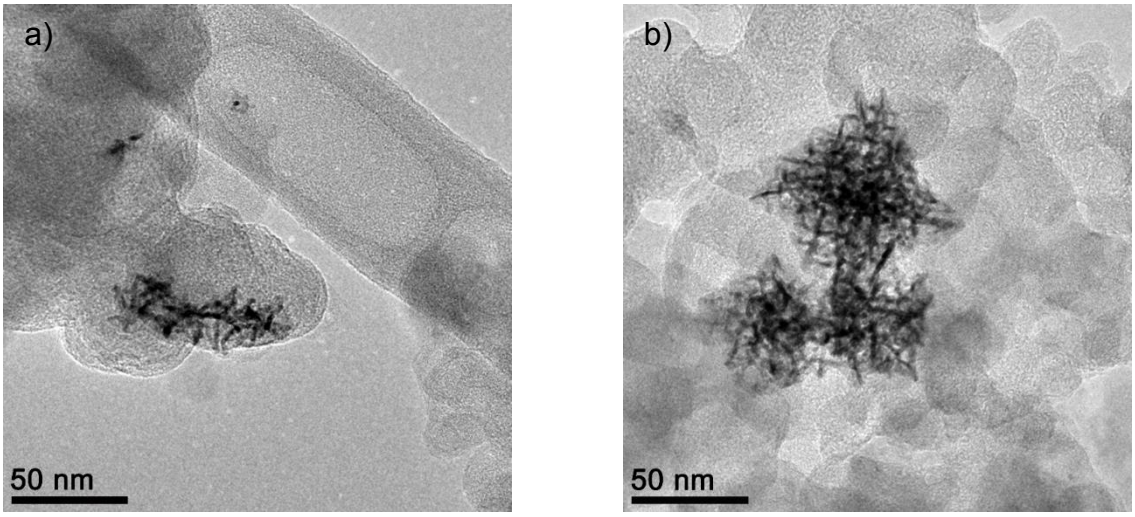

Figure S16. TEM images of the carbon black supported catalysts: (a) OSN/C and (b) HSN/C catalysts.

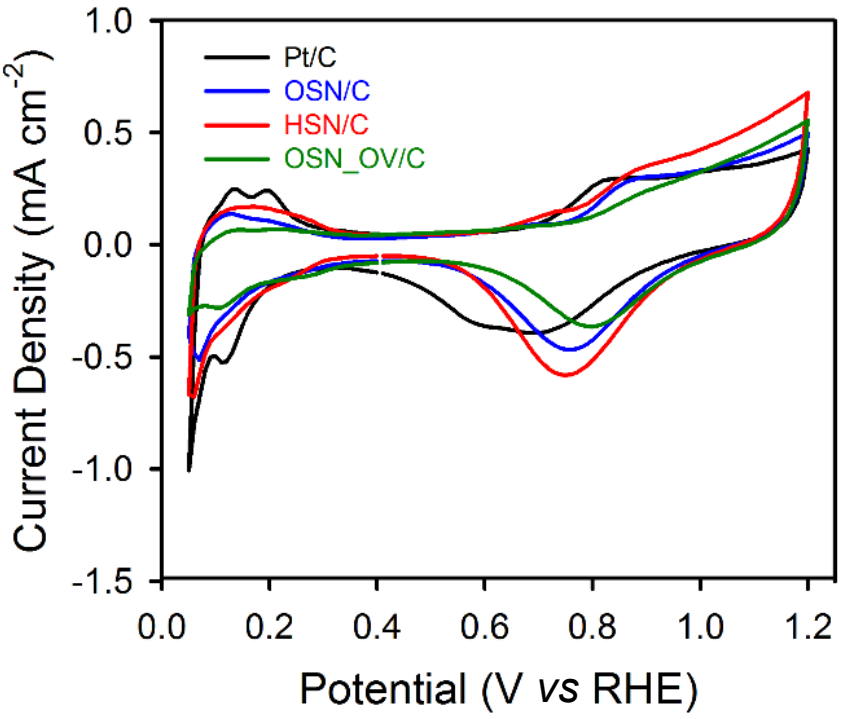

Figure S17. Cyclic voltammogram of nanocatalysts: Pt/C, OSN/C, HSN/C, and OSN_OV/C catalysts in N_2-saturated solution at a scan rate of 50 mV s^{-1}.

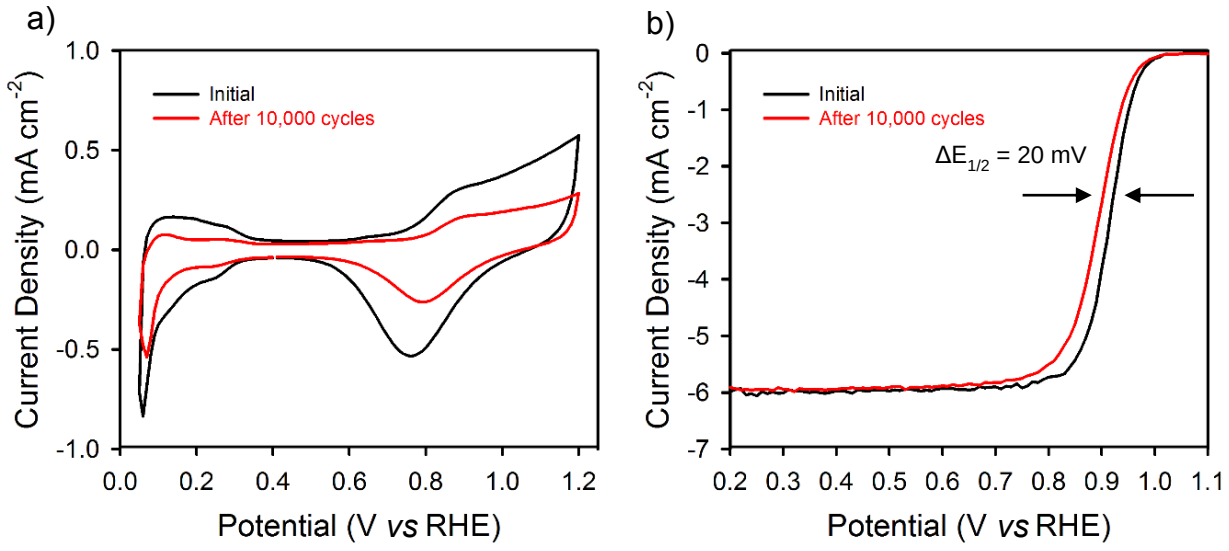

Figure S18. Electrochemical stability of the HSN/C catalyst. (a) Cyclic voltammogram and (b) the ORR polarization curve before and after potential cycling between 0.6 and 1.0 V *vs* RHE for 10,000 cycles at a scan rate of 50 mV s^{-1}.

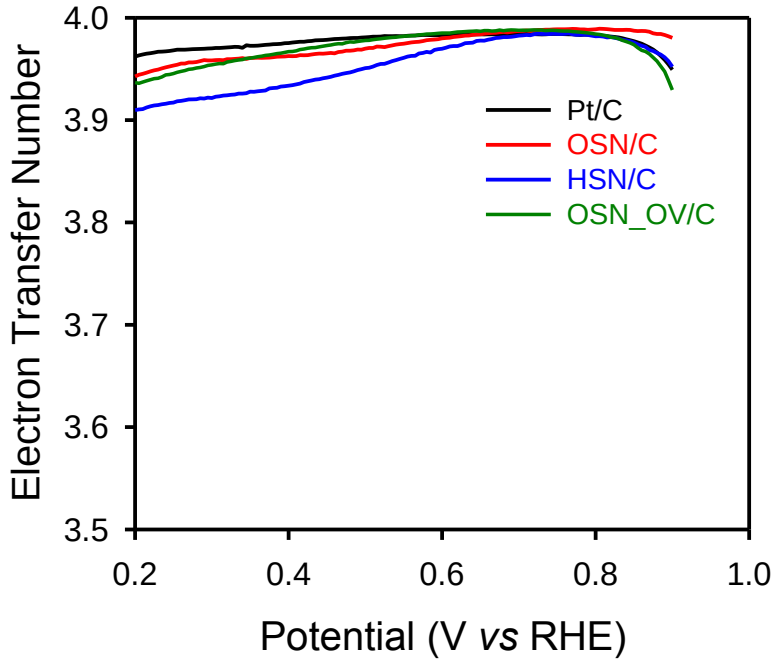

Figure S19. The electron transfer numbers of Pt/C, OSN/C, HSN/C, and OSN_OV/C catalysts during ORR. From the rotating ring disk electrode (RRDE) measurements, we could assess oxygen reduction reaction (ORR) pathway of the four catalysts (OSN/C, HSN/C, OSN_OV/C, and Pt/C). From the measured ring currents, the H_2O_2 yields and electron transfer numbers of the four catalysts were calculated. The electron transfer numbers of all catalysts are close to four, strongly suggesting that the ORR on these four catalysts proceeds *via* a direct four-electron process.

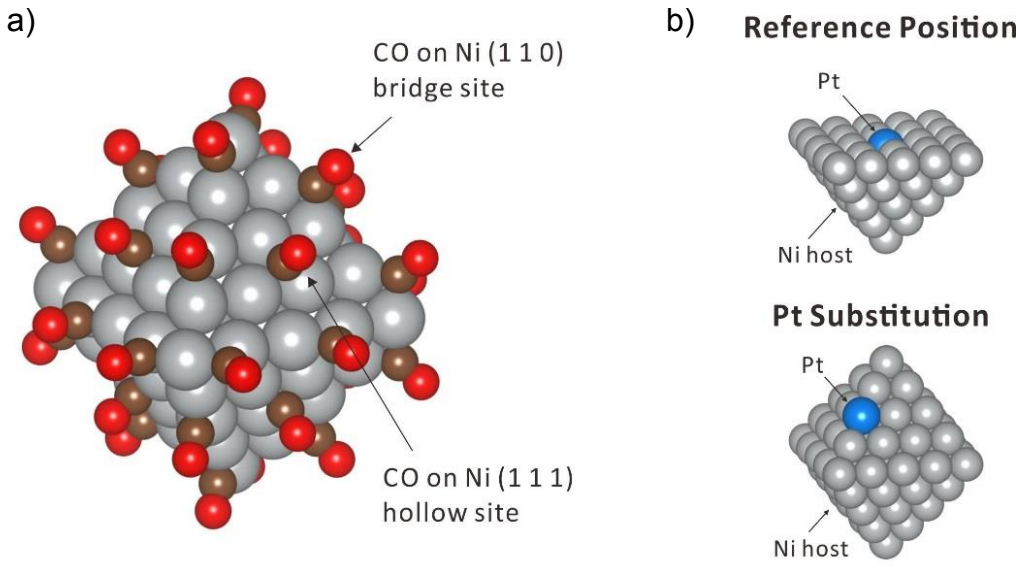

Figure S20. Geometrical details of the DFT calculations. (a) CO adsorption sites for the model Pt-Ni nanoparticle. 24 COs occupied the bridge sites on the Ni (110) sites and 8 COs filled up the remaining hollow sites on the (111) plane. (b) Reference position for relative energy calculations. Each position was substituted with the Pt atom and the total energy was compared to that of the reference position.